Development of the monitoring software for the JEDI polarimeter (JePo) optimization at COSY

Master Thesis

Submitted by

Irakli Lomidze

Master of Science in Engineering Technology

Agricultural University of Georgia

March 2023

Tbilisi, Georgia

Supervisors: Prof. Dr. Zaza Metreveli; Dr. Irakli Keshelashvili

Abstract

The matter-antimatter asymmetry in the Universe might be understood by investigating charged particle Electric Dipole Moments (EDM). A permanent EDM of a subatomic particle violates time reversal (T symmetry) and parity symmetry (P symmetry); Hence, it violates CP symmetry and can be a strong indication for physics beyond the Standard Model. The Jülich Electric Dipole moment Investigations (JEDI) collaboration is carrying out a project using the COSY accelerator for the direct measurement of EDM for protons and deuterons. For this matter, a heavy LYSO crystal based designated calorimetric polarimeter was developed. For the precise energy measuring purposes, the raw values needs calibration. In the scope of this thesis - the software was developed, which enables users to automatically generate calibration coefficients for the energy values and get the most precise measurement the one can get. The UX/UI is specially fitted to the experiment. However, the algorithm is more general and with a little modification the software can be extended and can be used by numerous analysis team - giving the opportunity of more automation in the accelerator physics.

Contents

Chapter 1

Introduction

One of the greatest questions for humanity is how the universe was created and why it is like this. The Big Bang theory models this process in a beautiful way - from the earliest known periods through its contemporary state.

According to this model the universe was very hot and dense at the time of its creation, implying the presence of equal amount of both - matter and antimatter. However, based on our observations, the universe consists only from the ordinary matter, which tells us that there must have been some asymmetry during the early stages of the Universe expansion - in a process called as Baryogenesis, in which matter and antimatter eventually annihilated to photons and neutrinos, leaving only a small amount of matter which led to the world that we see today.

In 1960s Standard Model (Later - SM) was introduced for describing origin of the elementary particles and for their interactions. SM states that disappearance of antimatter is outcome of the violation of the fundamental symmetries: Charge (C), Parity (P) and Time (T). Although, SM satisfies many fundamental experimental results, the source of CP violation in SM in not enough to explain such a big difference between matter and antimatter. So, it is remained as a challenge to understand the origin of this asymmetry. Since SM of elementary particle physics failed to provide a satisfactory explanation, there is a motivation to go beyond the Standard Model.

The CP symmetry breaking property of the Electric Dipole Moment (Later - EDM) makes it an interesting candidate for an additional source of CP violation. Despite the SM prediction of EDM of being very small or even zero, it is yet to be proven.

The Juelich Electric Dipole Investigation (JEDI) collaboration aims at the measurement EDM for protons and deuterons with a statistical sensitivity of 10^{-29} e cm in a storage ring based experiment, which can push science beyond the standard model and help us understand the universe better.

Chapter 2

Theoretical Background

2.1 Baryon Asymmetry

Symmetries are the fundamental concepts of physics, they are connected to the conservation of laws, such as: energy, momentum etc. We will discuss the 3 of SM symmetries below, which plays crucial role for understanding matter-antimatter issue. These symmetries are:

1. Charge (C) - Transformation, which switches all particles with their corresponding antiparticles. Thus, changing sign of all the charges.
2. Parity (P) - When the physical processes develop equally if spatial coordinates are inverted with respect to origin of the coordinate system.
3. Time (T) - Particle behaves similarly in the reverse of time

It was assumed that symmetries are held in every aspect of physical process. However, in the 2^{nd} part of the 20^{th} century it was proven otherwise - Chien-Shiung Wu performed experiment on ^{60}Co, that proved P symmetry violation in the weak interaction.

After P violation, CP invariance was considered to be held, until James Cronin and Van Fitch showed kaon decay violets CP symmetry. After this fact, even weaker symmetry was introduced - which combined all these 3 symmetries, called CPT theorem. Up until now, no process has been found that violets CPT symmetry.

As already stated, as far as we can see, the amount of matter exceeds the amount of anti-matter. Series of measurements have been done on Cosmic Microwave Background (later - CMB) spectrum, which have been summarized in the baryon-photon density ratio:

$$\eta = \frac{n_b - n_{\bar{b}}}{n_b + n_{\bar{b}}} \approx \frac{n_b - n_{\bar{b}}}{n_\gamma} = (6.08 \pm 0.09) * 10^{-10}$$

The SM also predicts this asymmetry. However, the ratio is 8 magnitudes less than the measured one:

$$\eta_{SM} \approx 10^{-18}$$

To explain the asymmetry between matter and anti-matter, Andrei Sakharov in 1967 defined three conditions that have to be fulfilled:

1. Baryon number violation - Without this violation, it would be impossible for a system to evolve from a state with no baryons into a state with baryons, as the system initially was in a state with a baryon number B = 0.

2. C and CP violation - If C and CP invariance were fully conserved, for each process that created a particle another process that created an antiparticle with the exact same probability would exist, and therefore also no baryon asymmetry could have developed.

3. Deviation from thermal equilibrium. In thermal equilibrium, the expected value of all physical quantities, are stable and it would be impossible for the system to transit from a B = 0 into a $B \neq 0$ state.

Although, The SM does comply to Sakharov's requirements on some level, the difference of SM predicted and measured ratio is too high and pushes us to seek of additional CP violation source - which can be particles' EDM.

2.2 Electric Dipole Moment (EDM)

Electric dipole moment (EDM) - $\vec{d}$ is defined as a permanent separation of charges in particle. It is the fundamental property of a particle, similar to the Magnetic dipole moment (MDM) - $\vec{\mu}$.

$$\vec{d} = \frac{\eta}{2}\frac{e}{m}\vec{s} = d\vec{s}$$
$$\vec{\mu} = \frac{g}{2}\frac{e}{m}\vec{s} = \mu\vec{s}$$

In these equations: e - elementary charge of the particle; m - mass; g and η - dimensionless scaling factors; $\vec{s}$ - spin of the particle (EDM and MDM is aligned parallel or anti-parallel to it).

The existence of the EDM is violating P and T symmetry, hense CP symmetry also.In order to see this, we can apply P and T transformation to the Hamiltonian describing EDM and MDM for a particle at rest in the external Electric and Magnetic field:

$$\bar{H} = -d\vec{s}\vec{E} - \mu\vec{s}\vec{B}$$
$$P : \bar{H} = +d\vec{s}\vec{E} - \mu\vec{s}\vec{B}$$
$$T : \bar{H} = +d\vec{s}\vec{E} - \mu\vec{s}\vec{B}$$

However, in case of C transform, all the vector quantities in the Hamiltonian are reverted, consequently - Hamiltonian is conserved for the CPT transformation.

2.3 Spin And Polarization

Since our experiment and analysis heavily depends on the beam polarization, it is important to give some proper definitions here. In order to talk about polarization, first we must discuss spin.

The spin of elementary particles, such as: quarks, electrons, muons etc.; as well as composite particles, such as: neutrons, protons J/psi mesons etc.can be described as an inherited angular momentum with values only given in full or half integers of the reduced Plank's Constant $\hbar$. Particles with half-integer spins are called fermions - Hence, all the quarks and leptons are fermions; On the other hand, particles with full-integer spin are called bosons.

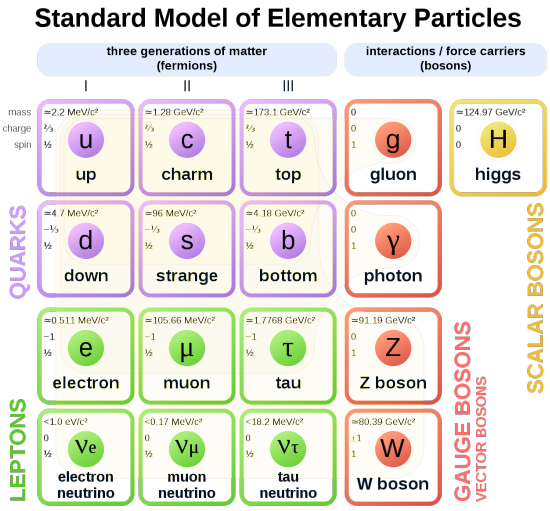

Figure 2.1: Standard Model of Elementary Particles

The spin is given by the quantum number s. In a quantum system spin defines quantization axis, which means that other vectorial properties, should be aligned with this axis - in our case: electric dipole moment (EDM). The spin can have different configurations relative to its quantization - z axis. For the particle with a spin of s, $(2s+1)$ different configurations can be found. This configurations are defined by quantum number m and can take values: $[-s, -s+1, ...s-1, s]$. Below is shown the configuration for $s = \frac{1}{2}$ and $s = 1$

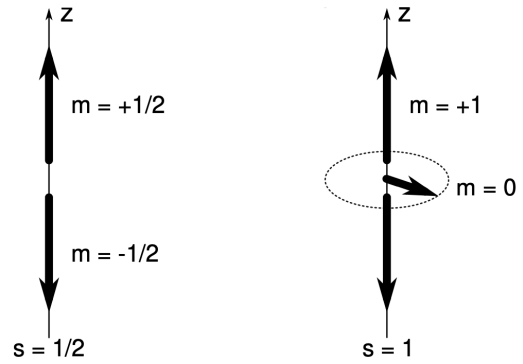

Figure 2.2: Configuration for spin for 1. Proton & 2. Deutron

In our experiment, it is next to impossible to approach each individual particle in the beam and talk about it's spin configuration. Instead, we can calculate polarization. In this scenario we are approaching the whole beam statistically - measuring the probability of finding a particle in the specific spin configuration.

let's discuss some examples:

• Assume we have a beam, with particles having spin $s = 1/2$. $N\uparrow$ particles in $m = +\frac{1}{2}$ configuration and $N\downarrow$ particles in $m = -\frac{1}{2}$ configuration. The vector polarization P_y will be

$$P_y = \frac{N\uparrow - N\downarrow}{N\uparrow + N\downarrow} = p\uparrow - p\downarrow$$

where $p\uparrow$ and $p\downarrow$ are probabilities of finding a particle with $m = +\frac{1}{2}$ and $m = -\frac{1}{2}$ respectively. From this equation we can conclude that polarization can change between -1 to 1 or from -100% to 100%.

$$-1 \leq P_y \leq 1$$

• Particles with spin $s = 1$, the beam can have: $N\uparrow$ particles with $m = 1$ configuration, $N\downarrow$ particles with $m = +1$ configuration and N^0 particles with $m = -1$ configuration. As a result, we would have the vector polarization:

$$P_y = \frac{N\uparrow - N\downarrow}{N\uparrow + N\downarrow + N^0} = p\uparrow - p\downarrow$$

However, since the $s = 1$ particles have a total - 3 configurations, the additional - tensor polarization has to be defined:

$$P_{yy} = \frac{N\uparrow - 2N^0 + N\downarrow}{N\uparrow + N^0 + N\downarrow} = p\uparrow - 2p^0 - p\downarrow = 1 - 3p^0$$

This leads to the restriction for possible tensor polarization values of:

$$-2 \leq P_{yy} \leq 1$$

When we combine the tensor and vector polarization restrictions, cause of the connection of them - we will get:

$$P_{yy} = 0 \Rightarrow -\frac{2}{3} \leq P_y \leq \frac{2}{3}$$

Chapter 3

Instrumentation

3.1 Cooler Synchrotron - COSY

The **Co**oler **Sy**nchrotron accelerator - **COSY** is located at the forschungzentrum Jülich in Germany and is being operated since 1993. The facility consists three main parts:

- A source that can produce polarized and unpolarized hydrogen H^- and deuterium D^- ion beams
- injector cyclotron JULIC (**J**ülich **I**sochronous **C**yclotron) - where particles are transfered from the source. This machine accelerates the ion beam to kinetic energies up to 45 MeV for H^- beams and up to 76 MeV for D^- beams
- The main cooler synchrotron storage ring COSY - particles are transferred from cyclotron

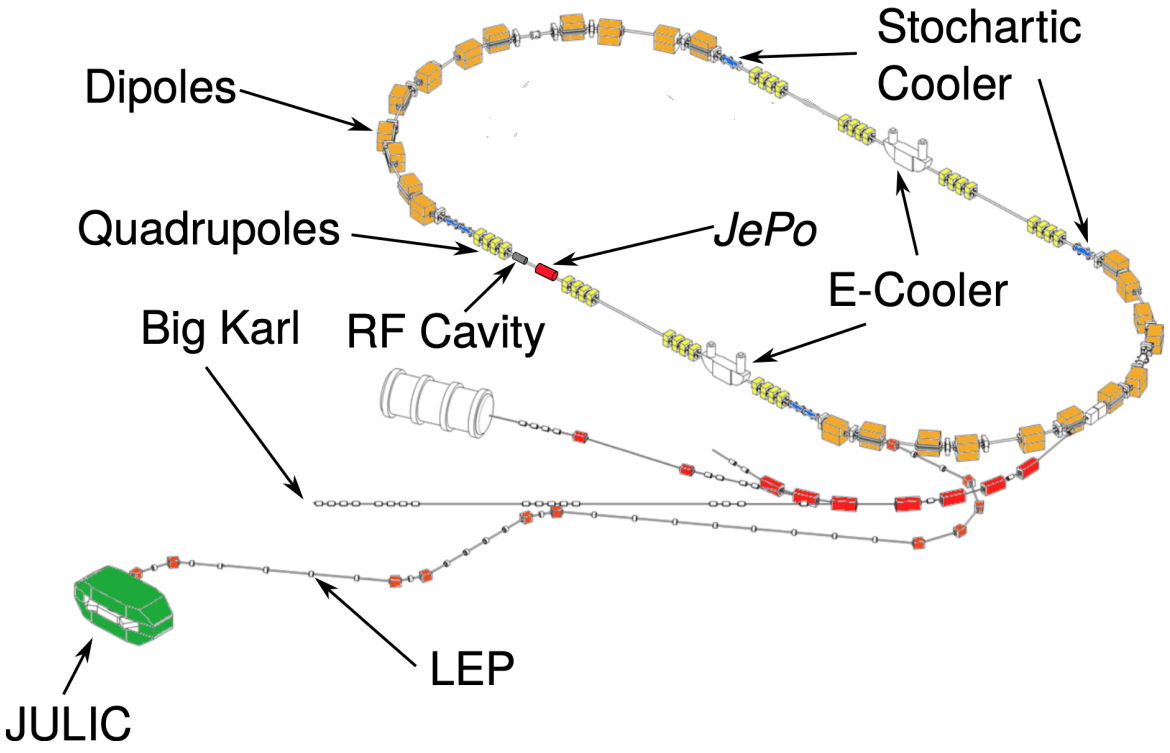

Figure 3.1: COSY Facility Schematics

To give the general understanding of the sub-devices:

- **Cyclotron** is a type of a accelerator, mainly used for accelerating non-relativistic charged particles (e.g. protons). The particles are accelerated by a electric field produced by high frequency alternating voltage and kept along the spiral trajectory by a static magnetic field.
  In the beginning, The particles are injected into the center. Than, because of the acceleration it goes not the circle trajectory, but the spiral, and are kept on the desired path by Lorenz force - produced by magnets. In order to always give the "kick" to the particles by RF, we need them to always be on some point at the exact time. So the specific frequency must be matched to the **Cyclotron Resonance Frequency**, which equals to:
  $$f = \frac{qB}{2\pi m}$$
  where: q - electric charge, B - magnetic field, m - relativistic mass

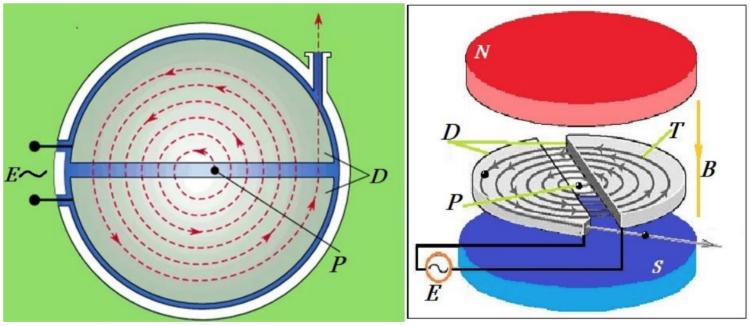

Figure 3.2: Cyclotron Schematics

- **Synchrotron** represents big circular tunnel, surrounded by various types of magnets, electro-magnetic lenses and accelerating devices. In reality, this type accelerator has many edges/sections, where each part is used for some specific purpose. Acceleration is mostly done on a straight part of the device via electric field; magnets (using Lorenz force) make sure that the particle beam stays in the designed orbit and electro-magnetic lenses focuses beam.

Returning to the COSY Accelerator - The circumference of the device is 184 m; it has 2 straight sections of 40 meters and 2 arcs with radius - 16.5 m. The facility is able to accelerate deuterons and protons up to a momentum of 3.7 GeV. For protons $E_{kinetic} \approx 2.8GeV$ and for deuterons $E_{kinetic} \approx 2.2GeV$ for deuterons. Acceleration is done in the RF cavity, which is installed in the one of the straight sections. The magnets that keep the beam in orbit are normal-conducting water cooled dipoles that can reach magnetic fields up to 1.58T. Groups of four quadruple magnets in a row form the beam optics - FODOs.

The feature that makes COSY stand out from the other synchrotrons is cooling. This option lets us reduce phase space of the beam by removing transverse momentum components. In order to get this advantage, 2 methods are used: **Electron Cooling** and **Stochastic Cooling**. Electron cooling is used up to 600 MeV, while Stochastic cooling starts from a 1.4 GeV.

To better understand **electron cooling**, let's dive deeper. 2 coolers are installed on a separate straight sections of the accelerator. A beam of electrons are injected in a short section of the ring with velocity equal to the beam. After this, electrons are scattered elastically with the beam particles and as a result, transverse momentum components of their

scattering partners are reduced. Finally, electrons are scattered out of the beam or are removed from the beat at the end of the electron cooler.

The stochastic cooling samples the beam positions in very fine packages as they enter through a so-called pick-up detector. Afterwards, the deviation from the ideal orbit is measured; the information is transferred to the device - called "kicker". When the beam travels along the ring and enters the kicker, a correction signal is applied - this signal is proportional to the measured pick-up. This way we are reducing the phase space of the beam in the both: transversal and longitudinal direction.

Another feature COSY provides is extraction point - using magnetic septum we can move the beam to the extraction line and to the 1 of the 3 experimental rooms. Must be mentioned, LYSO based polarimeter development was done at the Big Karl experimental room.

3.2 Polarimeter - JePo

The EDM search requires a polarimeter with: high efficiency, large analyzing power and stable operating characteristics. With typical beam momenta of about 1 GeV/c, the scattering of protons or deuterons from a carbon target into forward angles becomes a nearly optimal choice of an alayzing reaction.

Based on these requirements JEPO polarimeter was developed and first used on COSY at the Forschungszentrum Jülich with 0.97 GeV/c polarized deuterons, a particle and energy suitable for an EDM search. The polarimeter is based on inorganic LYSO crystals read out using silicon photomultipliers (**SiPM**s) immediately behind a thin plastic scintillator (also with SiPM readout) used for particle identification via energy loss. These detectors eventually observe proton or deuteron scattering from a thick carbon target. The polarimeters consists of 52 LYSO detector modules, aranged in 4 symmetric blocks (up, down, left, right + corner crystals). The entire assembly is 1.3 m long and is placed in a straight section of COSY.

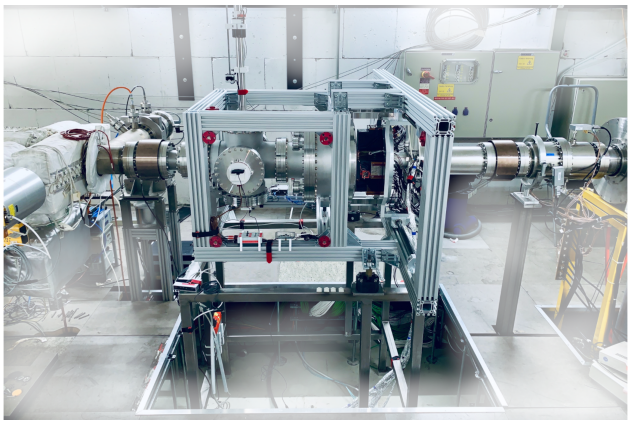

Figure 3.3: JEPO polarimeter in COSY

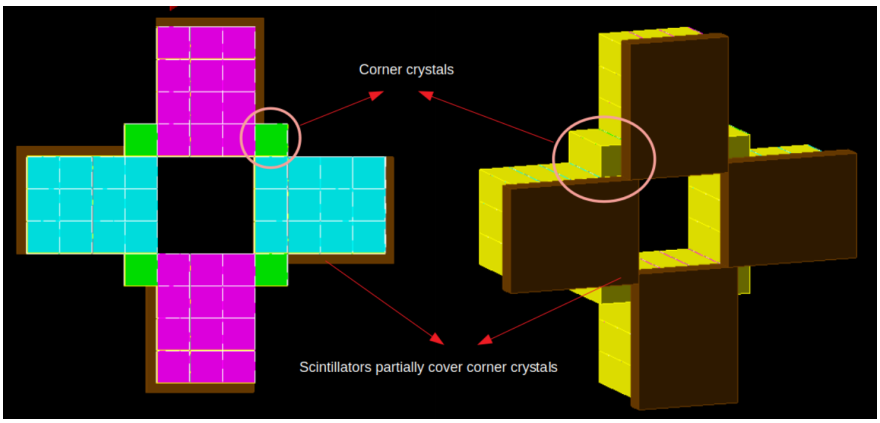

Figure 3.4: Detector module's configuration

Understanding the working principle of the JEDI polarimeter - JePo: The beam goes from left to right, passing the carbon block target suspended from above by movable support rod. The rod can be moved remotely in order to be remove the target during the beam injection and acceleration. The beam-side target edge is placed on the beam center line to reduce systematic errors in the polarimeter asymmetry due to any displacement from the center. Nowadays, beam bumps are used at COSY to displace the beam at the target position by about $3mm$ while running the data acquisition.

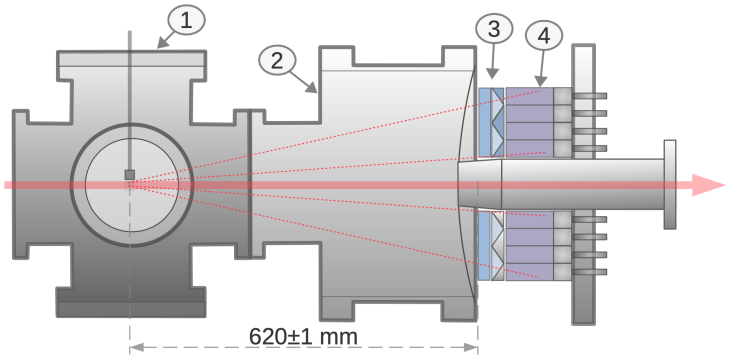

Figure 3.5: JePo schematic

The target chamber expands from the target location, until it reaches the exit window, which is made of $800\mu m$ stainless steel. Here scattered beam particles encounter a plastic scintillator energy-loss detector.

In the last part, particles enter heavy inorganic **LYSO** scintillators, where their remaining energy is absorbed.

Readout of the scintillator light is obtained using **SiPM** chips, mounted directly onto the read end of the LYSO crystals and the edges of the plastic scintillator. In this way we are minimizing the space along the beam line devoted to the polarization measurement and reducing external fields that may disturb EDM measurement.

It is crucial for the polarimeter to be efficient and extract as much information about changes in the polarization as possible. This efficiency is defined as the ratio of the number of events used to calculate the polarization to the number of beam particles consumed by an interaction with the polarimeter. Ideally, all the stored beam particles should interact with the

polarimeter target.

In order to see the polarimeter efficiency, we have made an observation on a beam and polarimeter count rate.

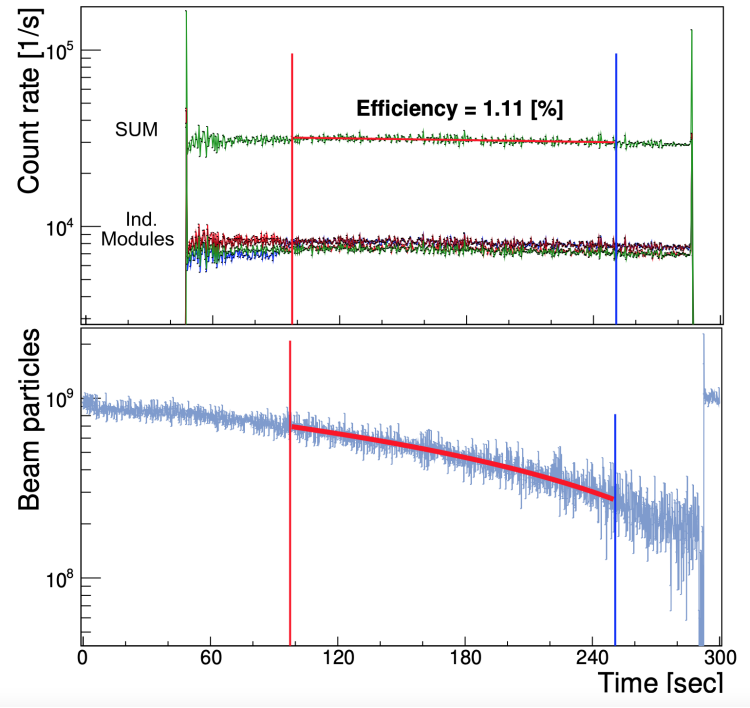

Figure 3.6: Polarimeter Efficiency

On this experiment, typical fills at the end of the electron-cooling time contained approximately 10^9 deuterons. The counting rates for the four quadrants of the polarimeter appear as colored traces on upper panel that are nearly flat for the data acquisition period. The green trace shows the summed count rate. The start of beam extraction onto the target generates a spike in rate. The declining beam current is shown as a blue trace in the lower panel that slopes steadily downward after the start of data acquisition. This start time also applies to the white-noise generator that brings particles in the beam to the polarimeter carbon target. The count rates are regulated through a feed-back loop to the white noise generator, and they remain steady throughout the store. The sum of the count rates and the loss of the beam current may be read from this output for any desired time interval. The ratio of total events within a time interval marked by the red and blue vertical lines divided by the loss of beam particles for the same interval is about 1.1%. This value meets the requirement needed for an EDM search on the proton at the level of 10^{-29} e cm.

The silicon photomultiplier or **SiPM** is a solid state photo detector, composed thousands of single-photon avalanche diodes (SPAD). The diodes are also called as microcells or pixels and are typically 10 to 50 μm in size. Each of the pixel is connected in parallel to the read out circuit, with their own quenching resistor and are operated in Geiger mode.

For setting the Geiger mode the ADPs are in reverse voltage bias above the breakdown voltage. In this mode a free charge carrier created or drifting in high electric field in the depletion region is accelerated such that it carries sufficient kinetic energy to create a diverging avalanche of electrons and holes, via impact ionisation. The APDs are in reverse voltage bias above the breakdown voltage to set it on Geiger mode.

The incidence of a photon on the SPAD generates a large electric signal due to breakdown. It must be noted that is possible to count each microcell triggered separately because the signal is the sum of all triggered SPADs. The SiPM operates at a low supply voltage - $27V$, it is robust, compact and insensitive to magnetic field which makes it an excellent choice for replacement of traditional photomultiplier tube (PMT) which requires voltage, greater than $1000V$.

Cerium-doped lutetium yttrium oxyorthosilicate crystals, or in short - **LYSO** crystals are used as a scintillation material. Talking about its main charasteristics: The light output is $32photons/keV$; The signal is fast - decay time is about $41ns$ at $420nm$ and it is nicely matched to the SiPM readouts; The crystals are not hygroscopic and they are dense - $7.1g/cm^3$ (densier materials increase probability of a gamma-ray interaction). As already mentioned, polarimeter consists of 52 of such crystals, where 48 of which are arranged in 4×3 arrays along the the four horizontal and vertical directions from the center. With this arrangement, we are covering scattering angles between 4° and 15°.

Figure 3.7: Detector Module's Parts

In the figure above we can see the module of detector with its sub parts:

1. LYSO Crystal
2. SiPM Array (8×8)
3. The housing and the mechanical system
4. wrapping with 3 layers: Teflon as a reflector, Tedlar to maintain light tightness, and Kapton for mechanical stability

The total length of the module is 14 cm. The crystal is coupled to a SiPM array via a 1 mm thick optical silicon interface. The SiPM readout array is the SensL J-series with $20\mu m$ pixels. The array's readout is made with a custom-made passive summarizer PCB, which adds up the charge from all 64 individual SiPMs. First the crystal is wrapped in $25\mu m$ white Teflon sheet, then it is wrapped in $25\mu m$ black Tedlar sheet. The entire assembly is held together by two strips of $25\mu m$ Kapton wrapped around the end of the LYSO crystal and pulled along the side, finally being held in place and tensioned with a circular wave-spring at the end.

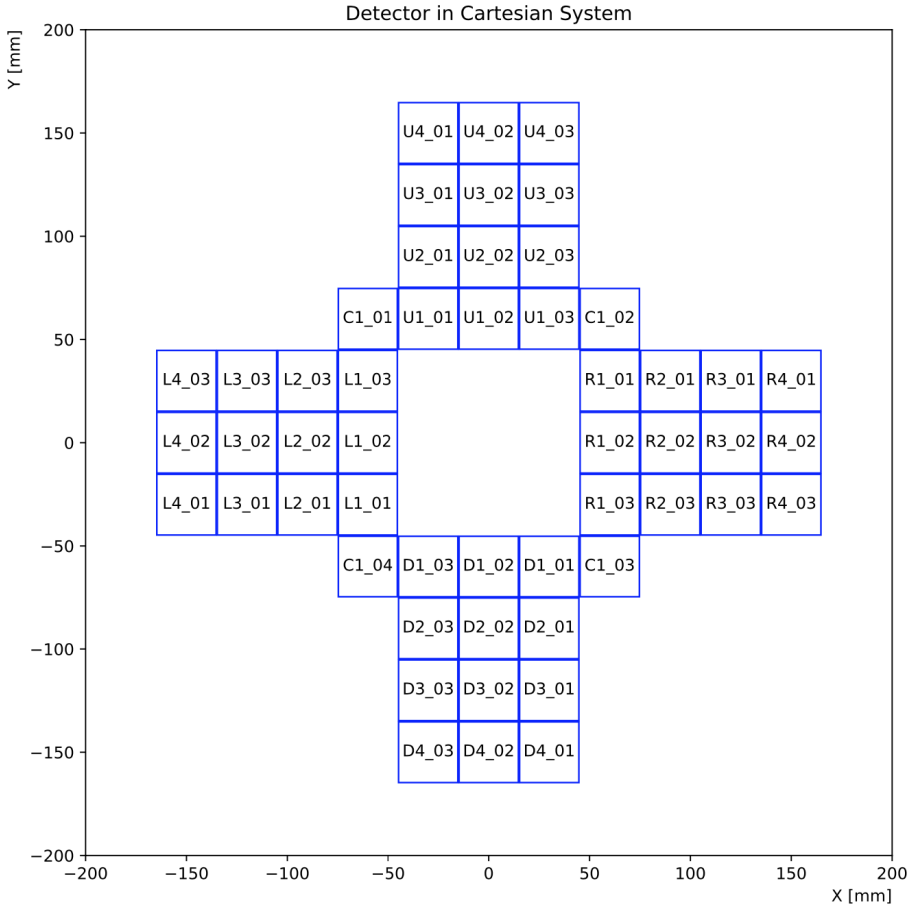

Figure 3.8: The arrangement of the ΔE detectors

Chapter 4

Experiment And Software Development

4.1 Experiment Methodology

It is considered that a storage ring might be used to extend the sensitivity of searches for an EDM by exploiting the realm of charged particle beams for which good statistical data can be obtained from specific polarimeters. The design of the storage ring must ensure the correct balance between electric and magnetic bending in the arcs so that we would have "frozen spin" - property where beam polarization direction and the particle velocity rotation speed are the same in the ring plane.

In order to reach the sensitivity goal of the EDM search of $10^{-29} e * cm$ on the proton, polarimeter must be able to detect rotations onto the vertical plane with value μrad using beam storage times at least $1000s$ accumulated during a total operating time of about one year. This means 10^{12} good polarimeter events. The beam will consist of 10^{10} particles per fill, split between counter-rotating beams. This implies trigger rates before event selection in the range of $10^6/s$, which must be recorded with minimal rate-dependent distortions. From this, the polarimeter should work best in trigger mode, responding to the information above some threshold level, rather than processing pulse height or timing information in order to make a more complex cut. Stability is also one of the crucial things, because we do not want to cause any changes in the vertical polarization between the beginning and the end of the beam. As a result, any cuts that define events should not be sensitive to the changes in the rates or the machine environment. It is likely, that final analysis of such data will involve corrections for systematic rate and geometry errors.

As a solution to this problem JEDI team has developed JePo (JEDI Polarimeter) - high-sensitive polarimeter which requires very high amount of events with small statistical errors within a reasonable running time. Moreover, as needed, analyzing power should be as large as possible - Analyzing power sets the scale of the sensitivity of the scattering to beam polarization. This leads to the choice of intermediate beam energies (momenta about 1 GeV/c), robust targets in the neighborhood of carbon or somewhat higher mass, and forward-angle elastic scattering as the ideal polarimeter concept. Usable scattering angles may range from the outer edge of the Coulomb-nuclear interference at a few degrees to roughly $\theta = 15°$. These features are almost independent of nuclear structure, arising mainly from the central and spin-orbit interactions between the projectile and the nucleus. This makes the isolation of elastic scattering from all other reactions less critical in the design, since inelastic scattering and even particle transfer reactions with low reaction Q-values show similar analyzing

powers. However, there is an exception: when deuteron breaks up and produces almost spin independent protons. It is for the best, if these protons can be removed before they reach any active detector element. It must be noted, that luckily for us - the best operating place for proton EDM search is at $p = 700.7MeV/c(T_p = 232.8MeV)$ where the analyzing power for $p + C$ polarimeter is near its maximum ($t_p = 210MeV$)

When doing polarization measurement one major task is to minimize systematic errors. When measuring asymmetric count rates with two detectors (such as L/R or U/D) we are eliminating problems associated with changes in the primary beam intensity. Two opposite vector polarization states with detectors to the left and right, which together generate four counting rates, can be combined to define a "cross-ratio" scheme that cancels many first-order errors with:

$$pA = \frac{r-1}{r+1}$$

$$r^2 = \frac{L_+ R_-}{L_- R_+}$$

L and R represents event rates for 2 sides of the beam.
+ and - represents polarization state of the beam.

These errors are often result of a broken geometric symmetry caused by positions or angle shifts in the beam or differences in the opposite detector responses. From the previously done research, we know that it is possible to calibrate the changes in the asymmetry measurements when geometric or rate-related errors arise. The choice of detecting forward-going reaction products allows a single systematic driving term

$$\phi = \frac{s-1}{s+1}$$

$$s^2 = \frac{L_+ L_-}{R_+ R_-}$$

can be used to estimate the corrections needed for both position and angle errors. From studies we know that errors on the signal below the 10^{-5} can be canceled. This is also very important for a successful EDM search.

The next crucial part of the polarimeter is it's target. The carbon block, which is used as a target, has demonstrated that it can be operated near a stored beam efficiently on the beam particles when measuring polarization. However, as every device, it has some disadvantage - the sampling of the beam is not homogeneous. As a solution, electron cooling was introduced. It is typically done $75s$ prior to any use of the beam and theoretically, it can make beam more uniform. As a result, reducing the chances of a significant polarization variation over the beam cross section.

4.2 Calibration Motivation

The COSY accelerator is a complex device and for every sub-device there are many factors to be considered during every stage of operation in order to get meaningful data. When talking about JePo and energy measurement acquisition credibility - we must dive deeper in to it's main sub-devices: **SiPM** and **LYSO Crystals**.

Every photo device has a noise which obeys Poisson distribution in the absence of photons. There are several factors affecting the noise in the SiPM. Main sources are: thermal noise and dark current.

- Thermal noise:
  Also known as Johnson noise or white noise, is the noise generated in the device due to the fluctuations in the voltage across a dissipative circuit such as: resistors caused by thermal motion of the charged carriers. The current generated due to thermal noise is given by:
  $$I = I_0 \exp \frac{\Delta E q}{K_B T}$$
  Where: K_B - Boltzmann constant; q - Charge; E - Electric Field; T - Absolute temperature; I - Current

- Dark Noise:
  This is a false positive triggers of the microcells in the complete absence of the photon. This is primarily due to thermal electrons generated in the active volume and the defects in the device. These defects and thermal electrons trigger the avalanche in high field region. This noise signal is identical to the signal generated by a photon and we consider this, only in the absence of photons. Since the amplitude of the noise signal is similar to that of a single microcell, while an actual signal involves triggering of multiple microcells, the noise can be neglected in the presence of a signal.

As stated, we need to deal with the noise and perturbation in energy measurement in order to get better results. Our approach for the energy calibration is to deal with the final outcome of the data instead of the finding and calibration each and every noise source.

4.3 Raw Data and Typical Spectras

The first of the data analysis is to acquire data. Luckily for us, huge amount of the data are observed and recorded during the experiment. So the only thing left for us is to access the database and fetch it.

The data readout is based on "dead-timeless" design using high-resolution sampling - 250 MSPS, 14-bit ADCs. Each pulse is divided into eight sampling regions: The first two of these, which precede the main pulse providing values for pedestal subtraction, and the other six are used to extract the amplitude.

The appropriate data bit is set from the pile-up detection algorithm provided by FADC firmware. The signal integral distribution can also be checked for evidence of pile-up in the measured signal.

Another thing to be considered is the possible time difference between the event recording for each and every individual module. To solve this issue, the clock signal is used to synchronize every module and event and they're being synchronised relative to the COSY machine RF. After this is done, events are recorded in a Linux server based program - capable of providing both online and offline analysis. As a remark, only the values of the eight integrals are transferred to the main processor and stored.

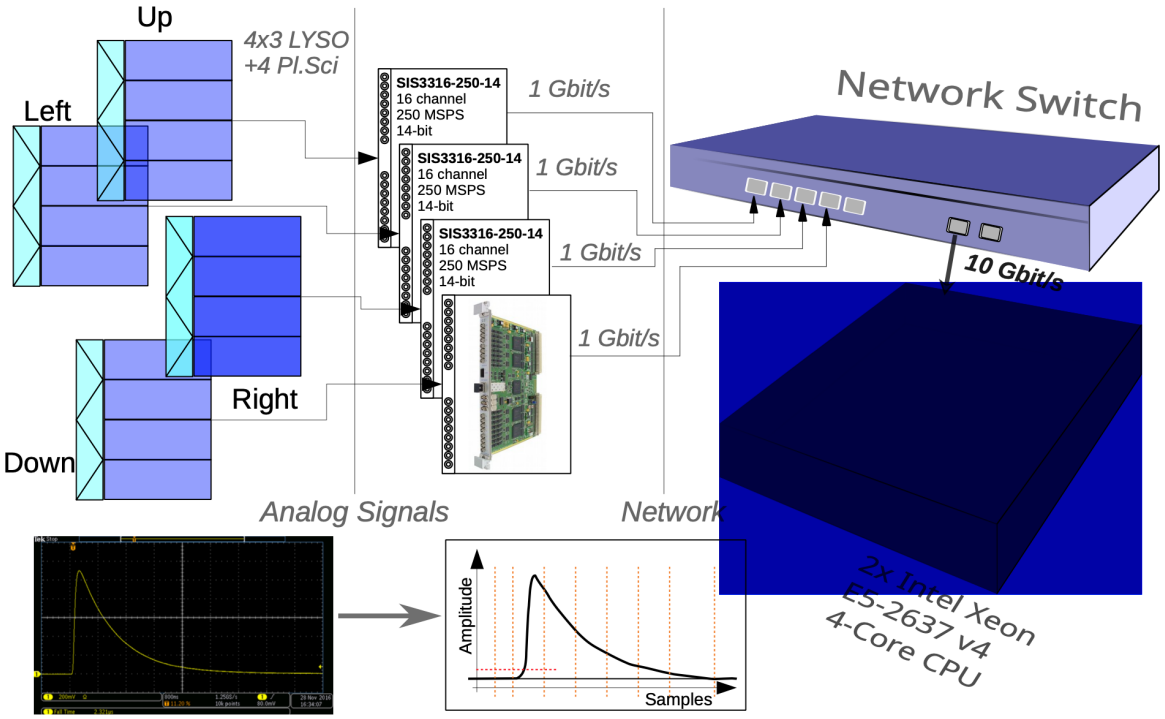

Figure 4.1: Data acquisition system

Considering the fact that the shape of the spectra always repeats itself in time, it will be very helpful to consider this for our analysis. Let's investigate single-event spectra for a row calorimeter detector. However, it is worth noting that spectras are not identical and have some variation.

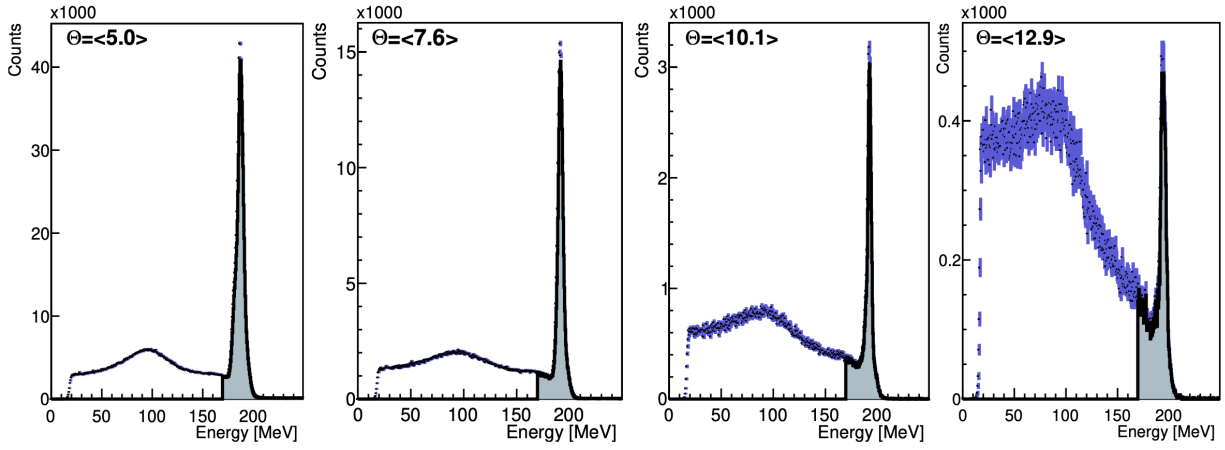

Figure 4.2: Typical Spectra Shape For 1 Row

From the image above, we can see pulse height spectra for one row of LYSO crystals shown in order of increasing scattering angle. The filled area indicates the fixed hardware threshold used during the event trigger. The cross section weighted scattering angle is also given for each spectrum. Each spectrum shows 2 main features:

- Elastic deuteron scattering from carbon - a narrow peak at high pulse height

- Proton/deuteron breakup + tail from the elastic peak - broader peak at lower energy

In addition to the LYSO crystals, there was also a general-purpose energy-loss scintillator mounted in front of the LYSO array. The resulting data obtained because from this installation can be seen on the figure below.

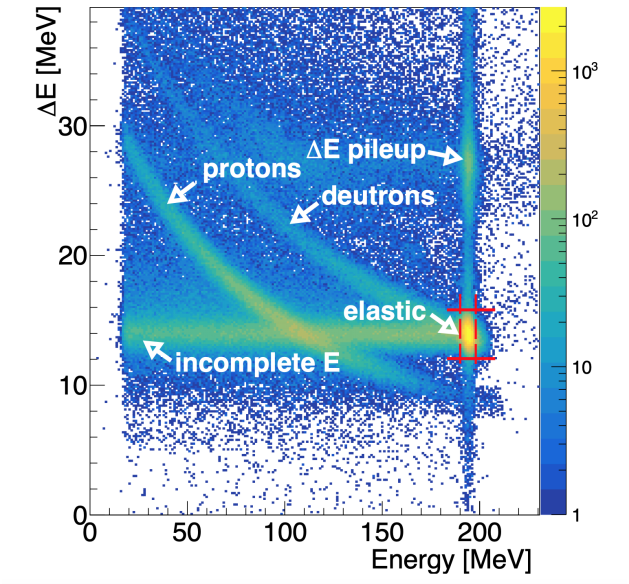

Figure 4.3: E over deltaE Overview

The figure represents 2D-Histogram of events as a function of LYSO pulse height on the X-axis and energy loss (ΔE) on the Y-axis. To better understand the figure, lets also describe every major point here:

- **The highest peak** seen on this 2D-Histogram is from elastic scattering, whose trails may be seen running parallel to both axes
- **horizontal/left** going line is due to the deuterons, interacting with the LYSO crystals and losing energy
- **vertically** we also have similar processes, including pileup in the energy-loss scintillator
- **The curved arc** starting from the elastic scattering peak represents inelastic deuteron reactions in the carbon target
- **A nearly parallel arc** just below it is due to protons. Midway along this arc is the main group representing protons from deuteron breakup in the carbon target.

4.4 Data Analysis And Calibration

Using the new software, we were able to fetch the data we wanted from the server and store it in a user friendly way. In the image below, we can see how the raw data of E over ΔE looks like on 2 dimensional histogram. We can see that the count and the shape definitely changes from module to module and also along the channels. The reason for this is that, depending on the position of the channel - scattering angle also changes; this leads to the different count rates on each channel and the different peak position on the histogram.

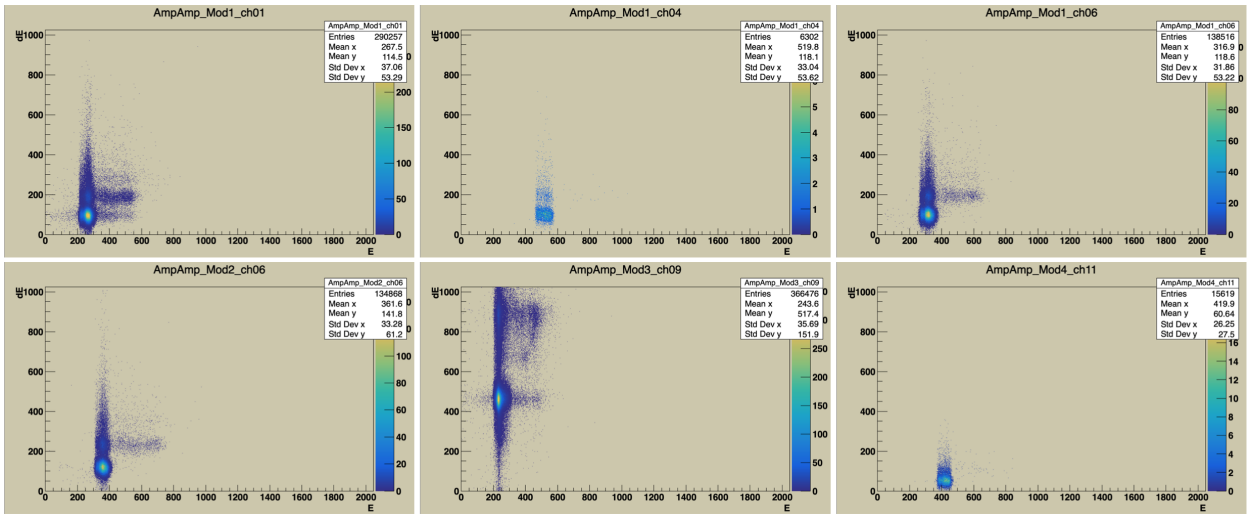

Figure 4.4: Raw Data Example on 2D Histogram

After acquiring the essential data for the analysis - it is time to filter it. Filtering process starts with projecting 2D histogram on ΔE (or y) axis. Next, we are fitting Gaussian function over the data and keeping the 3σ region. Finally, we are projecting filtered 2D histogram data on E (or x) axis for further analysis.

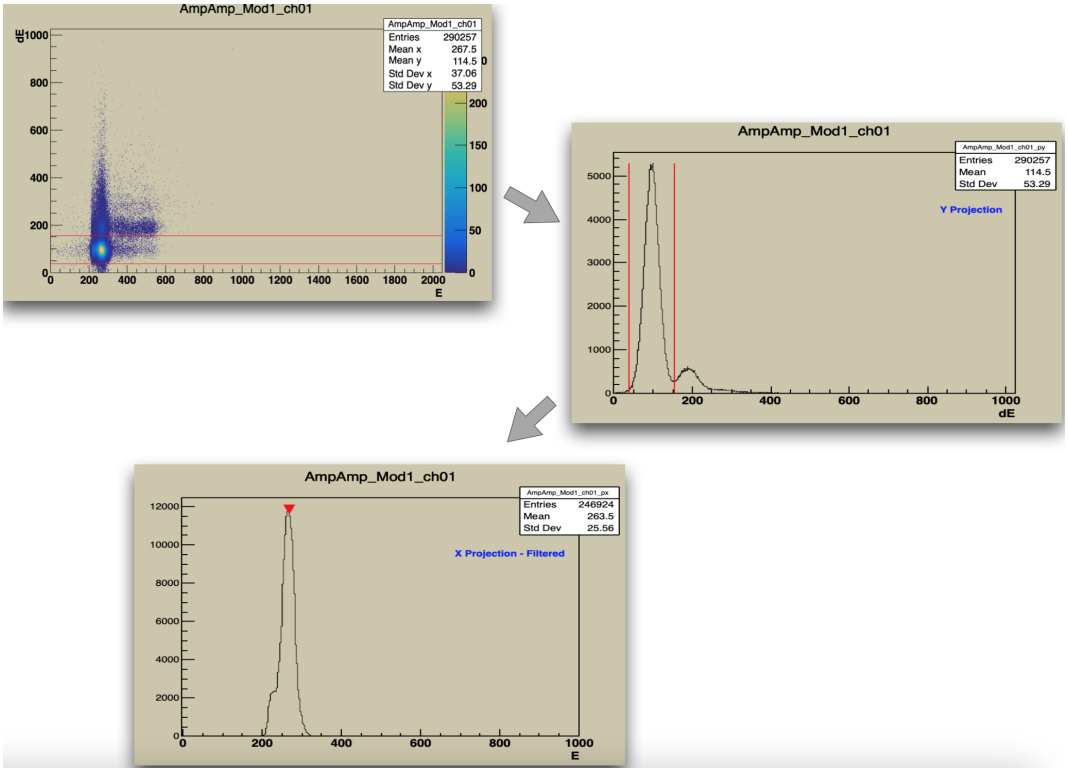

Figure 4.5: Data Filtration

After this filtration approach proofed correct, it was time to use it for every channel. Initially, the idea was to filter every module and channel data based on the one "sample source" - by getting the cutting ranges for filtration. This approach could decrease the computing power requirement and time. However, after further investigation, it became clear that every data source was unique and required individual approach. The proof of the current conclusion

can be seen below: The fixed cutting ranges (red lines) does not always return the peak fully inclusive range.

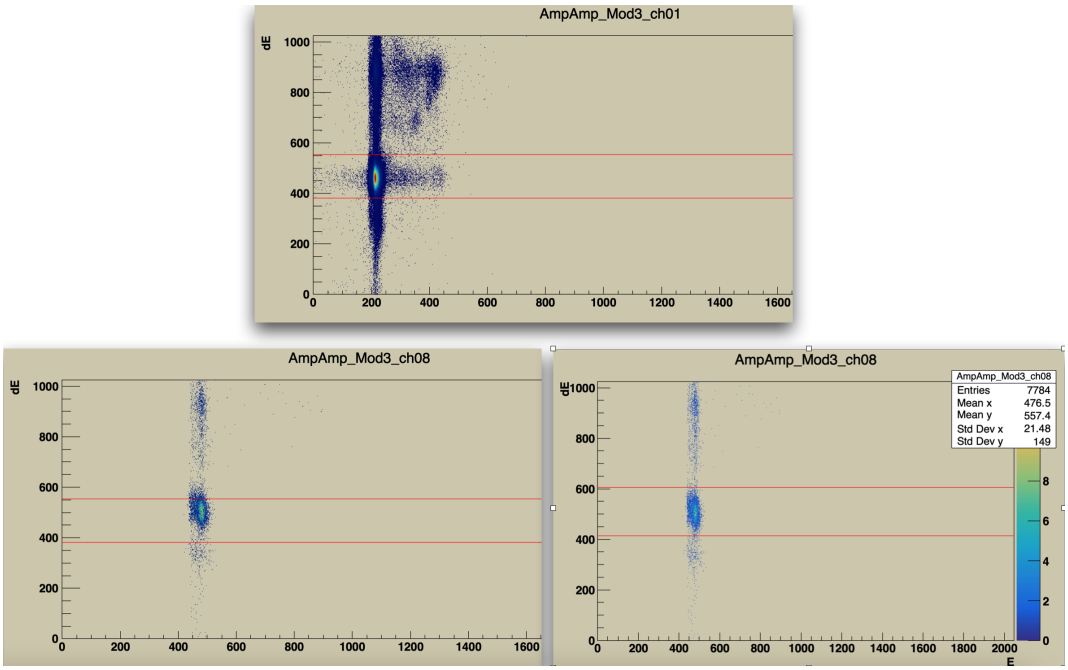

Figure 4.6: Filtration Issue

Presented evidence clearly states that not only event count differs from channel to channel, but peak position moves as well - making it impossible to filter every source based on one. Consequently, we are calculating data filtering ranges by analyzing every channel. To sum up, general scheme of the code will be presented down below:

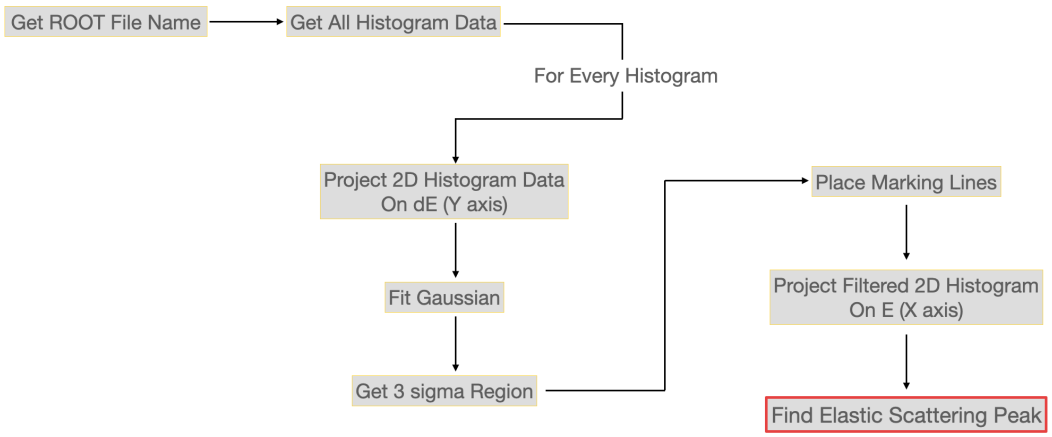

Figure 4.7: General Scheme Of The Filtering

As the filtration is done, the next step is to find peak values for every channel, which will be the energy calibration coefficients for JePo.

Finding the elastic scattering peak precisely is the most important task and to make it happen we are using some knowledge from physics to construct the most effective algorithm for our case. Firstly, we know that elastic scattering peak should have the highest energy

value on our scale. Hence, we are starting scanning from the highest energy values to the lowest (from right to left). As soon as we get the lower value than the previous one, we are testing it for the critical point - without it, we can not be sure whether or not this point is actually peak maximum, or just a data error from the sensor. To check it we are looking to the neighbour points and analyzing slope consistency. For the better visualization, there is a schematic block below; Moreover, example of peak finding consistency for few runs.

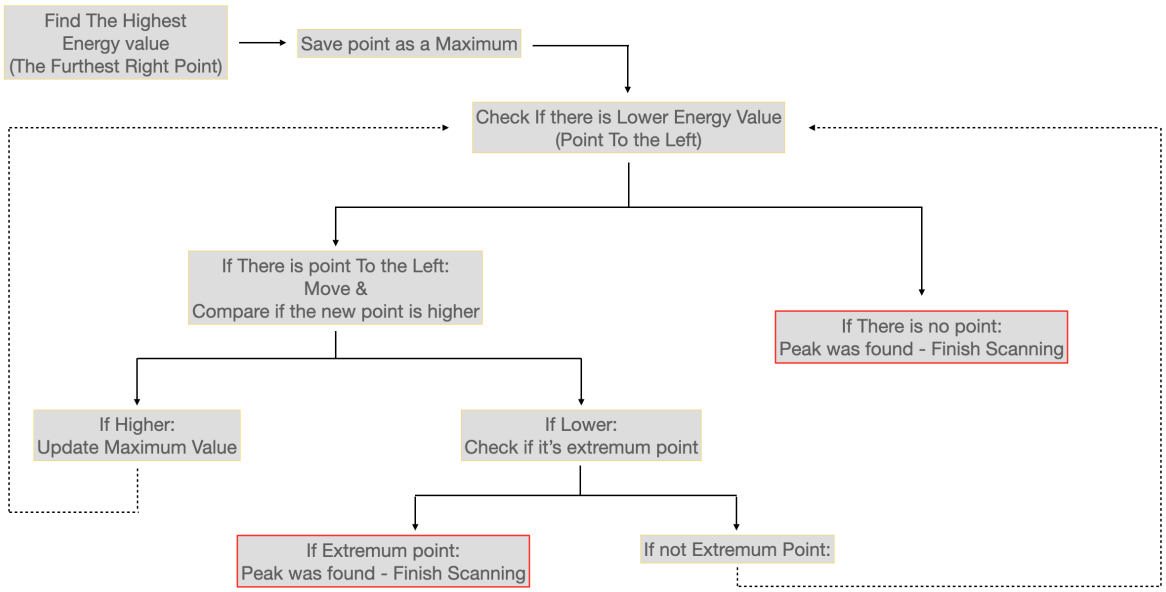

Figure 4.8: Peak Finding Algorithm

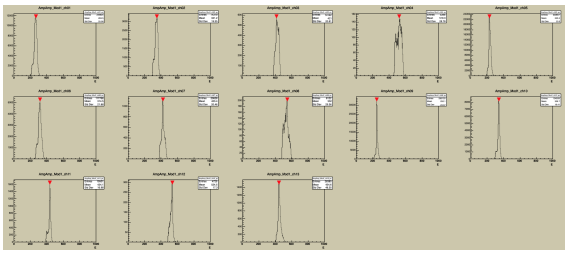

(a) Run 5803

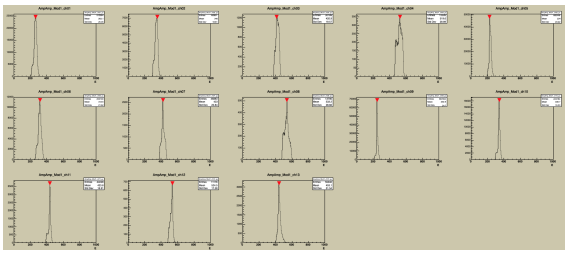

(b) Run 5804

Figure 4.9: Peak Recognition Consistency Example

After managing to find every channel's calibration coefficients, we are presented 2 choices:

- Analyze and calibrate data automatically after finishing every run;
- Find pattern/correlation for the calibration coefficient and apply it without recalculating every time.

The second approach is certainly orders of magnitude faster option and seems as a better choice. However, it can be useless if the correlation cannot be established and fitting function can not be found within the reasonable amount of sample data; or similarly - χ^2 would be unacceptable for the experiment. To investigate the situation 51 consecutive valid run points were taken for every channel. The result showed that, even though the device temperature did not have sudden changes and it had continuous pattern over the runs - energy calibration coefficients not only did not remained constant, they had substantial change of values.

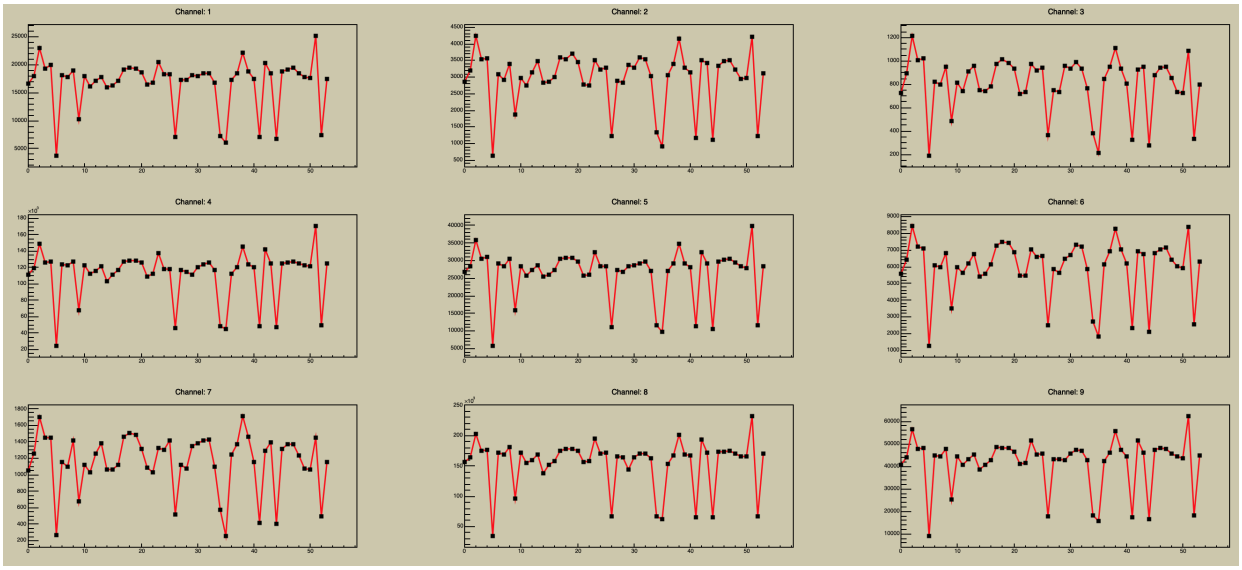

Figure 4.10: Calibration Coefficients Over Run

To investigate whether or not it is possible to calibrate coefficient without recalculating every time, first thing to do is the linear fitting. The Fitting was done for every channel, and the results are:

Table 4.1: Linear Fit Of Calibration Coefficients

Ch №	NDf	p_0	p_1	χ^2
1	52	17088.7 ±1210.33	-11.8431 ±39.3685	1.05719e+09
2	52	3054.98 ±224.989	-3.02664 ±7.31824	1.3.65315e+07
3	52	850.4 ±62.6671	-1.7153 ±2.03838	2.83416e+06
4	52	113120 ±8019.18	-34.1596 ±260.841	4.64094e+10
5	52	26998.5 ±1911.65	-18.9702 ±62.1807	2.63733e+09
6	52	6084.41 ±456.707	-4.6332 ±14.8554	1.50529e+08
7	52	1210.45 ±92.5975	-1.94839 ±3.01193	6.18792e+06
8	52	157692 ±11027.8	-96.908 ±358.703	8.77656e+10
9	52	42297.5 ±3022.5	-19.7012 ±98.3132	6.59293e+09
10	52	8539.06 ±634.284	-7.05268 ±20.6315	2.90345e+08
11	52	1751.86 ±139.252	-2.01296 ±4.52947	1.39942e+07
12	52	7607.76 ±529.409	-4.99931 ±17.2202	2.02269e+08
13	52	146665 ±10355	0.984143 ±336.818	7.73829e+10
14	52	45806.1 ±3284.68	18.1282 ±106.841	7.7863e+09
15	52	6653.19 ±501.874	5.81753 ±16.3245	1.81776e+08
16	52	1721.32 ±132.916	1.33025 ±4.32336	1.27496e+07
17	52	90259 ±6202.52	-43.6406 ±201.75	2.7764e+10
18	52	24186 ±1678.7	-1.58841 ±54.6035	2.03374e+09
19	52	4541.45 ±331.887	1.89278 ±10.7953	7.94925e+07
20	52	6.1250.56 ±95.3103	1.40236 ±3.10017	6.55581e+06
21	52	55702.1 ±3841.66	-8.55712 ±124.958	1.06509e+10
22	52	12337.7 ±854.049	-2.09941 ±27.7798	5.26394e+08
23	52	2304.31 ±162.855	0.372556 ±5.29721	1.91403e+07
24	52	755.719 ±53.8533	0.137107 ±1.75169	2.09301e+06

Ch №	NDf	p_0	p_1	χ^2
25	52	4246.72 ±292.275	-0.255003 ±9.50686	6.16494e+07
26	52	170995 ±12214.9	77.0266 ±397.314	1.07677e+11
27	52	37665.1 ±2694.52	18.0159 ±87.6449	5.23972e+09
28	52	11553.6 ±838.182	8.2316 ±27.2637	5.07017e+08
29	52	1786.54 ±126.544	0.296131 ±4.11612	1.15566e+07
30	52	160140 ±11402.1	96.7755 ±370.877	9.3824e+10
31	52	67112.2 ±4777.68	43.6791 ±155.404	1.64733e+10
32	52	13773.8 ±980.952	12.6308 ±31.9076	6.94451e+08
33	52	2149.18 ±150.231	0.691976 ±4.88659	1.62879e+07
34	52	99049 ±7014.95	47.0656 ±228.176	3.55137e+10
35	52	50567.4 ±3619.44	48.9309 ±117.73	9.45429e+09
36	52	9709.01 ±687.351	6.64894 ±22.3576	3.4096e+08
37	52	2273.85 ±159.262	1.74866 ±5.18033	1.8305e+07
38	52	10316.6 ±729.143	9.72605 ±23.7169	3.83682e+08
39	52	48484 ±3359.72	-6.96764 ±109.282	8.14617e+09
40	52	12693.8 ±879.629	0.0793215 ±28.6118	5.584e+08
41	52	2105.09 ±145.021	0.195578 ±4.71712	1.51778e+07
42	52	1594.36 ±110.826	0.632704 ±3.60486	8.86402e+06
43	52	59857.7 ±4156.17	-11.5921 ±135.188	1.24662e+10
44	52	17448 ±1214.39	-1.27982 ±39.5007	1.0643e+09
45	52	2504.17 ±173.802	0.435296 ±5.65328	2.17999e+07
46	52	837.511 ±57.3541	-0.0402516 ±1.86556	2.37397e+06
47	52	51442.3 ±3641.99	-4.49964 ±118.463	9.57245e+09
48	52	13538.6 ±955.099	-0.335315 ±31.0666	6.58329e+08
49	52	2332.54 ±164.268	-0.0476844 ±5.34316	94738e+07
50	52	834.23 ±57.9441	-0.245588 ±1.88476	1.2.42307e+06
51	52	11525.4 ±818.677	-2.34077 ±26.6292	4.83694e+08

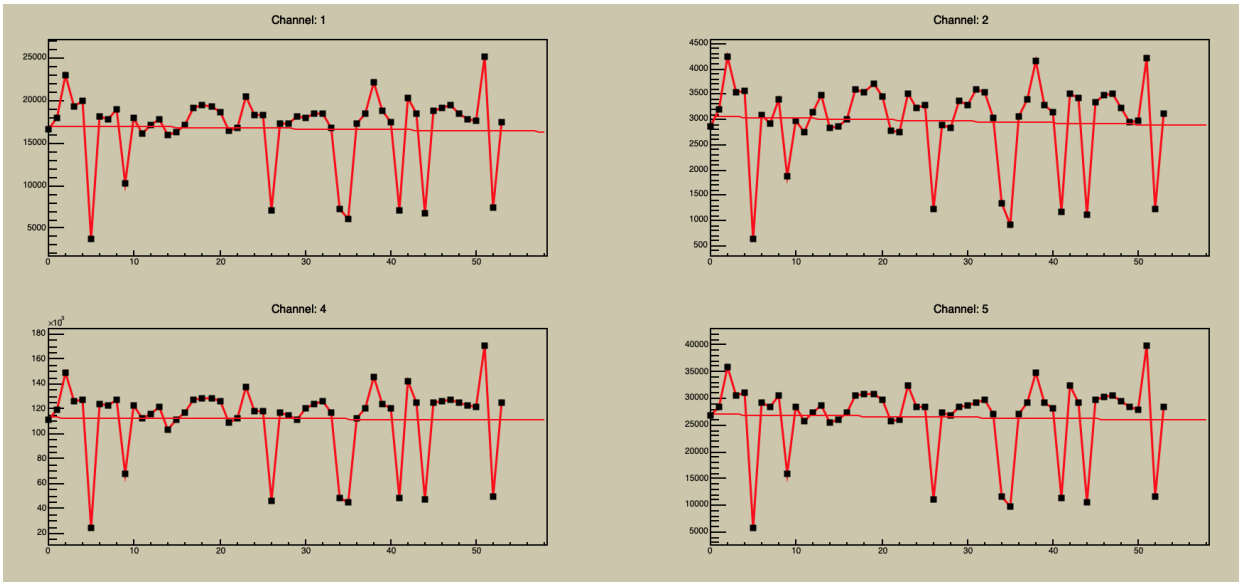

Figure 4.11: Fit Calibration Coefficients Over Run 1

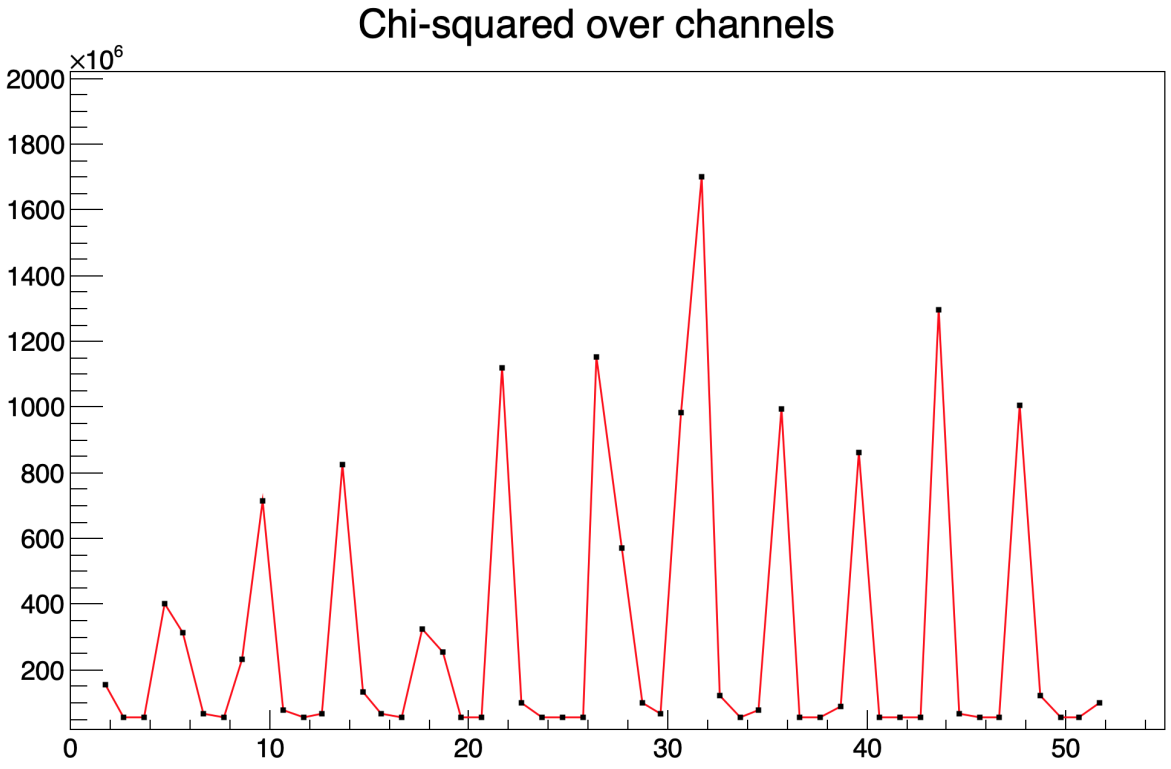

Figure 4.12: Chi-Squared Of Channel's Fit

The linear fit visualisation shows that the calibration coefficients are more or less around the fitted function. However, the deviation from it seems disturbing. For this matter, it is required to observe the χ^2 values. The numerical values are higher than order of 6 and they vary dramatically over the channels - all of this giving the hint that it is impossible to get the coefficients for further runs without analysing them as well.

4.5 User Interface

As the software starts, user is requested to enter the root file name storing the run data. Afterwards, graphical User Interface (GUI) is presented, showing: raw data with cut lines for filtering, filtration results via ΔE and peak value for the chosen/default channel. Moreover, user is presented action bar, giving options to: Navigate through modules and channels; Move energy peak manually if considered to be wrong; Generate the peak/coefficient value table and show all peaks simultaneously on a new canvas. New window gives user options only to navigate through channels/modules and generate calibration coefficients.

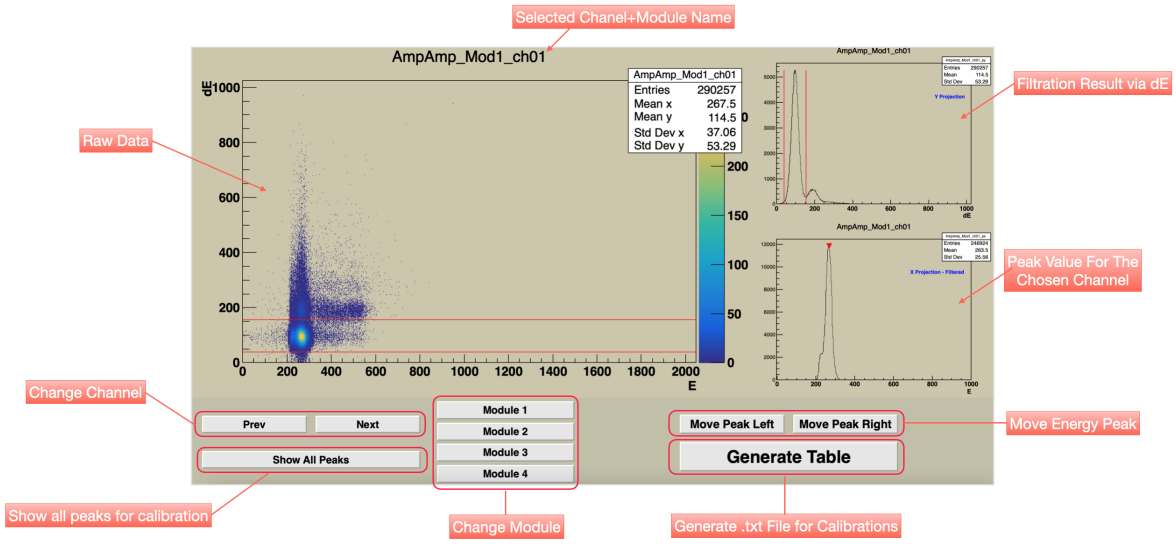

Figure 4.13: UI Screen 1

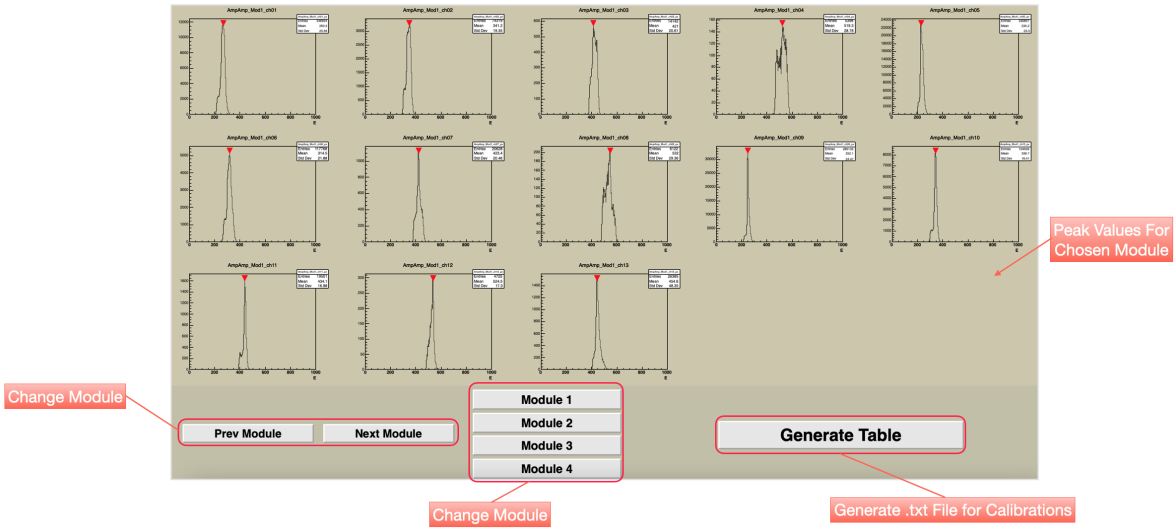

Figure 4.14: UI Screen 2

Chapter 5

Summary

In order to get the high precision energy values from the Jedi Polarimeter, SiPM and LYSO crystal obtained values must be calibrated. As part of the master's thesis, the software was developed to generate calibration coefficients automatically.

The software has been tested on data obtained from the 2021 experiment and has proven to be success. For now, the software is utilizable only in a offline mode - requires user to feed the data. However, with a little modification it can be used in an online mode - automatically fetching data and generating calibration coefficients.

Chapter 6

Appendix

Run Numbers

5397	5398	5399	5400	5402	5403
5404	5405	5406	5407	5408	5415
5419	5420	5429	5430	5431	5433
5434	5435	5436	5443	5444	5445
5446	5447	5451	5452	5453	5454
5455	5456	5457	5458	5459	5461
5462	5463	5464	5465	5466	5467
5478	5479	5480	5483	5484	5485
5486	5487	5488	5489	5491	5512

Calibration Coefficients over Run

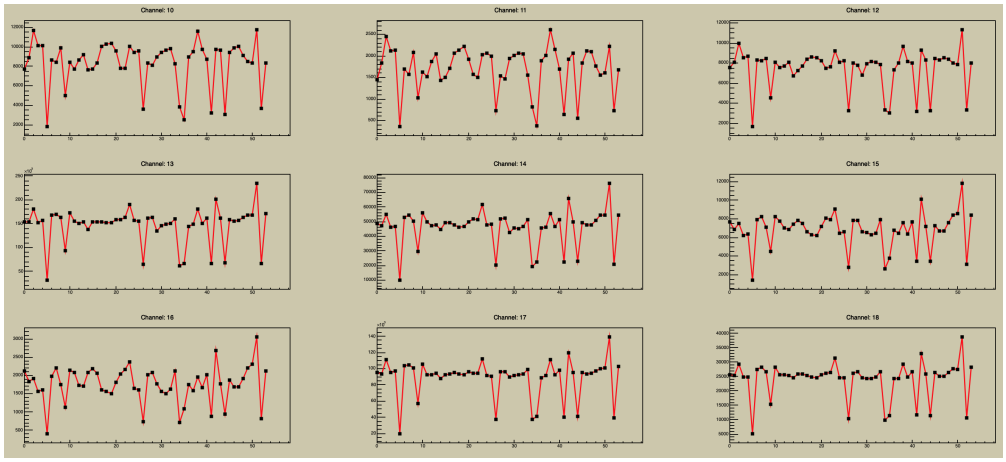

Figure 6.1: Calibration Coefficients Over Run - 2

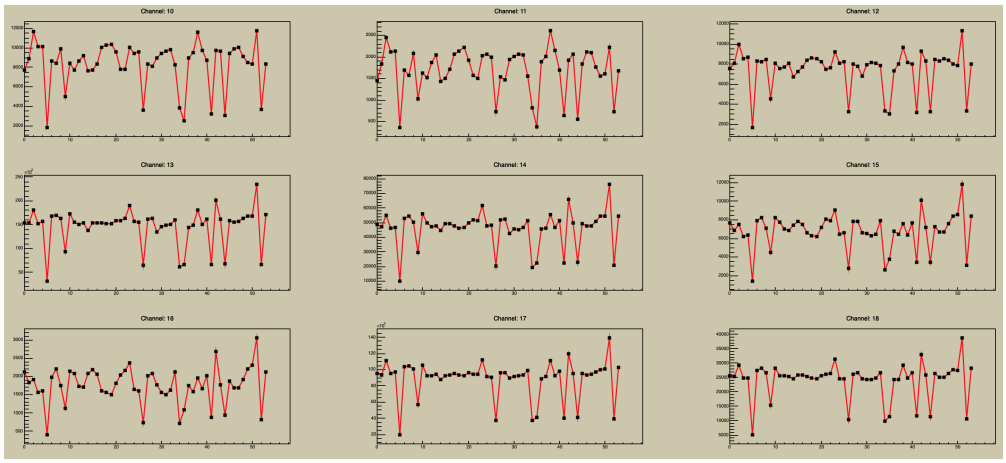

Figure 6.2: Calibration Coefficients Over Run - 3

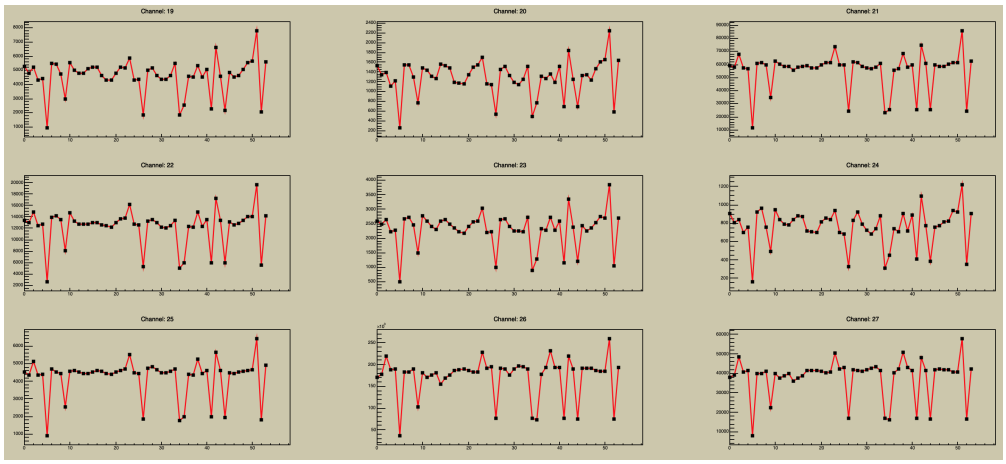

Figure 6.3: Calibration Coefficients Over Run - 4

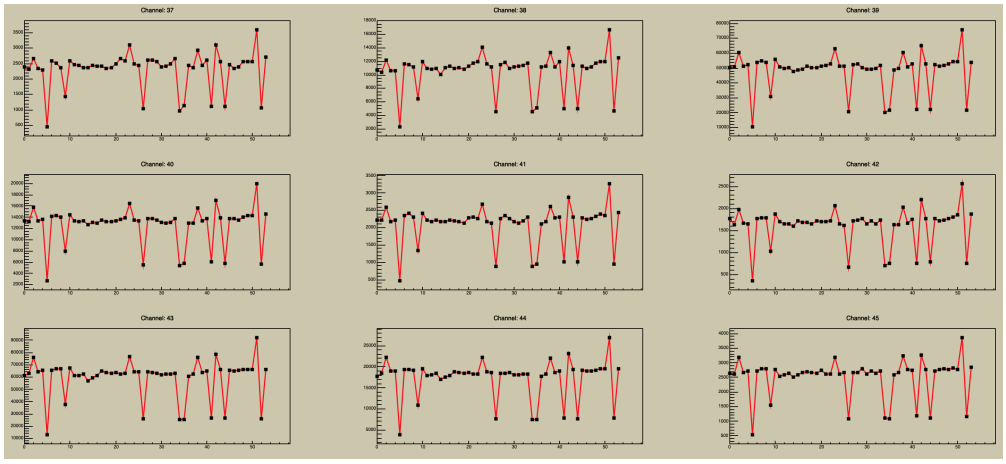

Figure 6.4: Calibration Coefficients Over Run - 5

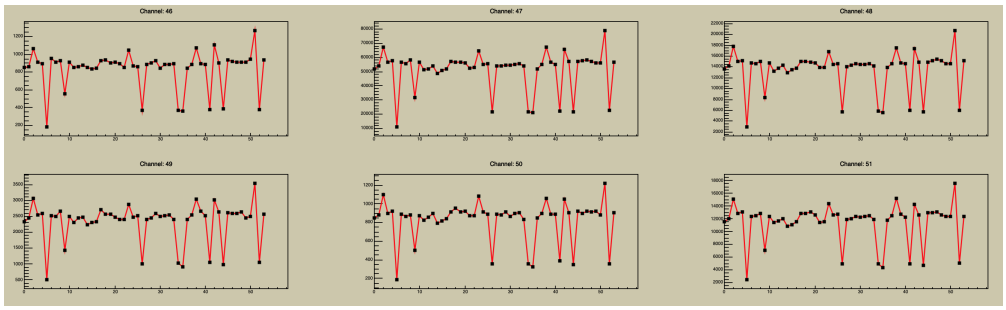

Figure 6.5: Calibration Coefficients Over Run - 6

Fit Calibration Coefficients over Run

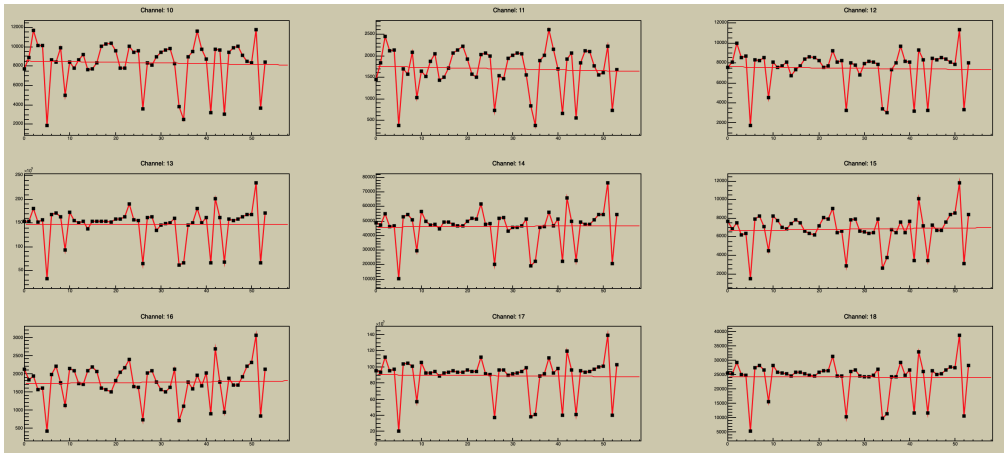

Figure 6.6: Fit Calibration Coefficients Over Run - 2

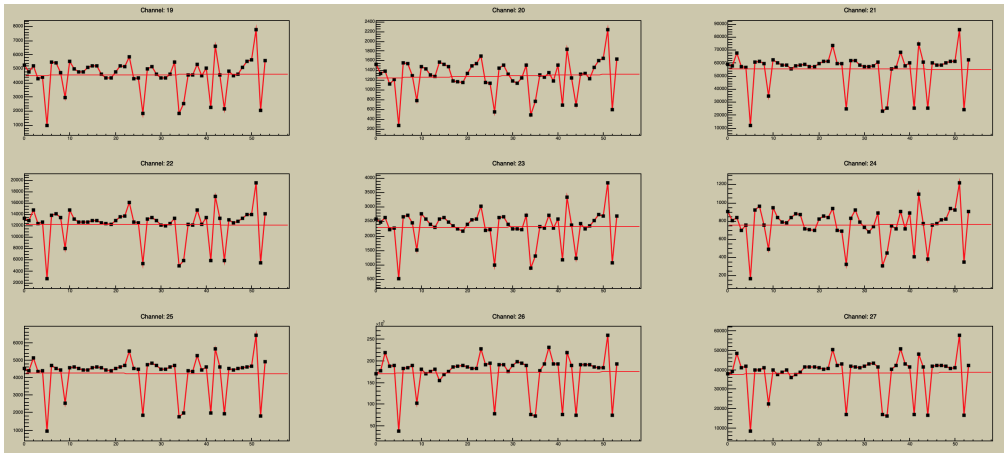

Figure 6.7: Fit Calibration Coefficients Over Run - 3

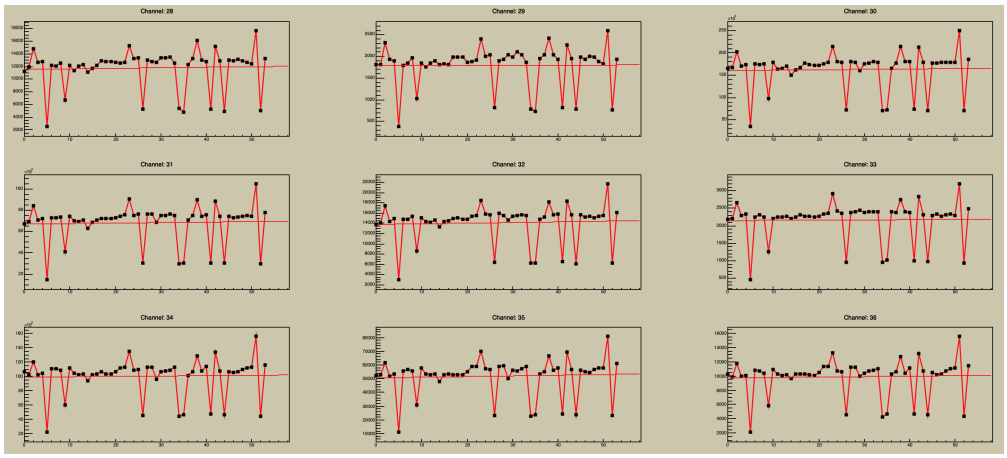

Figure 6.8: Fit Calibration Coefficients Over Run - 4

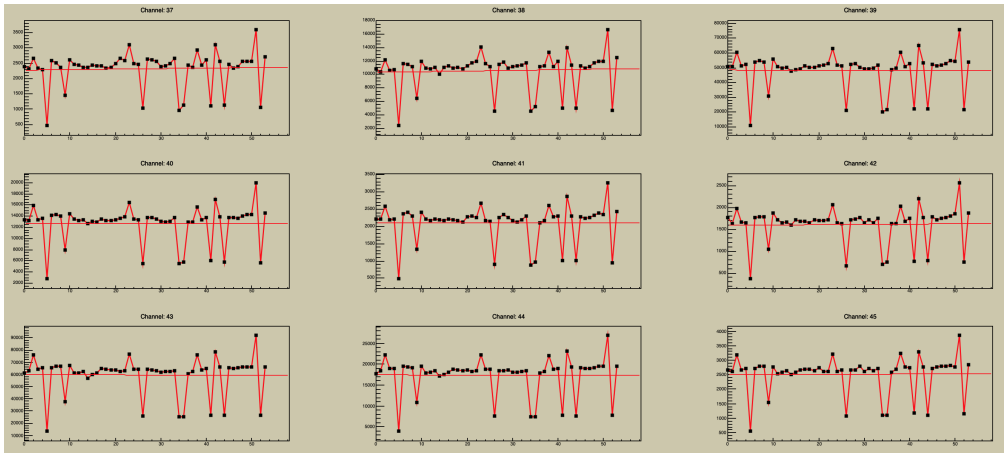

Figure 6.9: Fit Calibration Coefficients Over Run - 5

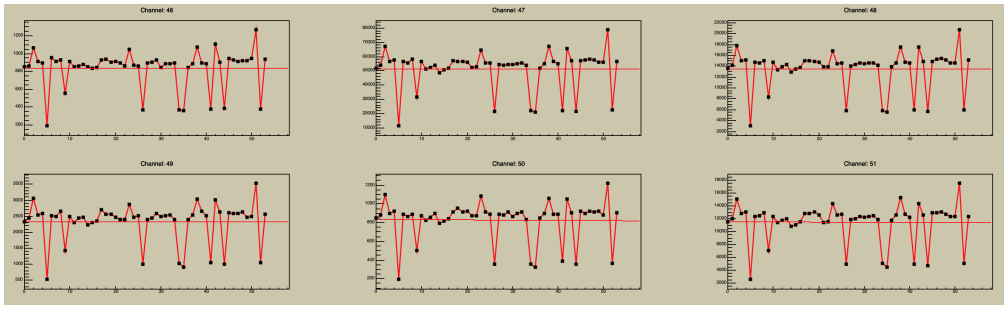

Figure 6.10: Fit Calibration Coefficients Over Run - 6

List of Figures

Chapter 7

Bibliography

1. JEDI Collaboration. Homepage. http://collaborations.fz-juelich.de/ikp/jedi/, 2019.
2. JEDI collaboration, A new beam polarimeter at COSY to search for electric dipole moments of charged particles, 2020
3. Fabian Müller, Polarimeter Development for Electric Dipole Moment Measurements in Storage Rings, 2019
4. Anoop Koushik, Characterization of the SiPM arrays for the JEDI polarimeter using a dedicated measurement setup, 2020
5. Jamal Slim, A Novel Waveguide RF Wien Filter for Electric Dipole Moment Measurements of Deuterons and Protons at the COoler SYnchrotron (COSY)/Jülich, 2018
6. Laurent Canetti, Marco Drewes, and Mikhail Shaposhnikov. Matter and Antimatter in the Universe. New Journal of Physics, Focus Issue on the Origin of Matter, Vol. 14 (095012), 2012.
7. W. Bernreuther. CP Violation and Baryogenesis, 2002.
8. A. D. Sakharov. Violation of CP Invariance, C Asymmetry and Baryon Asymmetry in the Universe. Pisma Zh. Eksp. Teor. Fiz., Vol. 5, Nr. 1, 1967.
9. Thomas Mannel. Theory and Phenomenology of CP Violation. In The 7th International Conference on Hyperons, Charm And Beauty Hadrons (BEACH 2006), volume 167 of Nuclear Physics B. Lancaster: Elsevier, 2006.
10. Dr. J. F. J. van den Brand. Discrete symmetries. Vrije Universiteit, Amsterdam, The Netherlands. Introductory Course.
11. F. R. Klinkhamer and N. S. Manton. A Saddle-Point Solution in the Weinberg- Salam Theory. Physical Review D, 30:2212–2220, 1984.
12. C. L. Oxley, W. F. Cartwright, I. Rouvina, E. Baskir, D. Klein, J. Ring, and W. Skillman. Double scattering of high-energy protons by hydrogen and carbon. Physical Review, Vol. 91, Nr. 2:419–420, 1953.
13. F. Abusaif et al., Storage Ring to Search for Electric Dipole Moments of Charged Particles - Feasibility Study, CERN-PBC-REPORT-2019-002, arXiv:1912.07881.
14. E. Fermi. Polarization of High Energy Protons Scattered by Nuclei. Il Nuovo Cimento, Vol. 10, Nr. 4, 1954.

15. H. Stein et al. Current Status of the COSY Electron Cooler (Jülich, Germany) . Atomic Energy, Vol. 94, No. 1, 2003.

16. N. Hempelmann. Polarization Measurement and Manipulation for Electric Dipole Moment Measurements in Storage Rings. PhD thesis, RWTH Aachen University, 2018.

17. F. Rathmann, A. Saleev, and N.N. Nikolaev, Search for electric dipole moments of light ions in storage rings, Phys. Part. Nucl. 45 (2014) 229

18. R. Maier et al. Cooler Synchrotron COSY. Nuclear Physics A, Vol. 626:395 – 403, 1997.

19. U. Bechstedt et al. Field Measurement of the Magnets for COSY - Jülich. In EPAC 92, Third European Particle Accelerator Conference, 1992.

20. D. Prasuhn et al. Electron and Stochastic Cooling at COSY. Nuclear Instruments and Methods in Physics Research A, Vol. 441:167 – 174, 2000.

21. H. Calen et al. Detector Setup for a Storage Ring with an Internal Target. Nuclear Instruments and Methods in Physics Research A, Vol. 379:57–75, 1996.

22. J. Pretz and F. Müller. Extraction of Azimuthal Asymmetries Using Optimal Observables. The European Physical Journal C, Vol. 79:47, 2019.

23. T. Kawabata et al. Isovector and isoscalar spin-flip M1 strengths in 11B. Physical Review C, Vol. 70:034318, 2004.

24. R. Brun et al. CERN-W5013: GEANT Detector Description and Simulation Tool. https://cds.cern.ch/record/118715?ln=en, 1994.

25. K. Ermisch. Search for Three-Nucleon Force Effects in Proton-Deuteron Elastic Scattering. PhD thesis, University of Groningen, 2003.

26. K. Sekiguchi et al. Complete Set of Precise Deuteron Analyzing Powers at Intermediate Energies: Comparison With Modern Nuclear Force Predictions. Physical Review C, Vol. 65:034003, 2002.

27. F. Abusaif et al. Feasibility Study for an EDM Storage Ring. arXiv e-prints, page arXiv:1812.08535, Dec 2018.

28. J. Pretz. Comparison of Methods to Extract an Asymmetry Parameter From Data. Nuclear Instruments and Methods A, Vol. 659:456–461, 2011.

29. Dr. William R. Leo. Techniques for Nuclear and Particle Physics Experiments, A How-to Approach. Springer-Verlag, 1994.

30. G. Audi, F.G. Kondev, M. Wang, B. Pfeiffer, X. Sun, J. Blachot, and M. Mac- Cormick. The NUBASE 2012 evaluation of nuclear properties. Chinese Physics C, Vol. 36, No. 12:1157–1286, 2012.

31. Jianming Chen, Rihua Mao, Liyuan Zhang, and Ren-Yuan Zhu. Gamma-Ray Induced Radiation Damage in Large Size LSO and LYSO Crystal Samples. IEEE Transactions on Nuclear Science, Vol. 54, No. 4:1319–1326, 2007.

32. S. Basile. Development of a High Precision LYSO Polarimeter for EDM Search at COSY Storage Ring . PhD thesis, Universit‘a degli Studi di Ferrara, 2019.

33. M. Urban et al. The New APD Based Readout for the Crystal BarrelCalorimeter. Journal of Physics: Conference Series, Vol. 587, 012043, 2015.

34. Units The NIST Reference on Constants and Uncertainty. The Deuteron Mass Equivalent in MeV. https://physics.nist.gov/cgi-bin/cuu/Value?mdc2mev, 2014.

35. N.P.M. Brantjes et al. Correcting Systematic Errors in High-Sensitivity Deuteron Polarization Measurements. Nuclear Instruments and Methods in Physics Research A, 664:49–64, 2012.

36. J. Pretz on behalf of the JEDI and CPEDM collaboration. Electric Dipole Moment Measurements at Storage Rings. In Proceedings of the Discrete 2018 Conference, Journal of Physics: Conference Series, 2019.

37. 2004 KVI Run With Plastic Scintillator and NaI Detectors. courtesy of E. J. Stephenson.

38. D.F. Nelson, A.A. Schupp, R.W. Pidd and H.R. Crane, Search for an Electric Dipole Moment of the Electron, Phys. Rev. Lett. 2 (1959) 492

Chapter 8

Acknowledgements

Firstly, I want give my sincere gratitude to my supervisors: Prof. Dr. Zaza Metreveli from the Agricultural University of Georgia (Tbilisi, Georgia, email: z.metreveli@agruni.edu.ge) and Dr. Irakli Keshelashvili from the Institute of Nuclear Physics (Jülich, Germany, email: i.keshelashvili@fz-juelich.de) who gave me instructions, guidance and support during my work.

I would like to express my deep appreciation to the Director of IKP - Prof. Dr. Hans Ströher and to Dr. Andro Kacharava for their valuable assistance and opportunity to write thesis at the Institute of Nuclear Physics (IKP) of the Forschungszentrum Jülich (Germany).

Moreover, I would like to thank Dr. David Mchedlishvili from SMART—EDM Laboratory (Georgia), who prepared me for the challenges during the thesis work.

Furthermore, I would like to thank all of the JEDI collaboration members for the friendly environment, inspiring conversations, valuable experience and shared knowledge.

Last but not least, I would like to thank Shota Rustaveli National Science Foundation of Georgia for the financial support (Document №JFZ_21_131) during my stay at Jülich, Germany.